A Framework for Peak Power Exceedances of High Power Microwave Radiators Applied to a Vircator Surrogate Model

**Mae AlMansoori[1, 3, *], Ernesto Neira[1], Sebastien Lallechere[2], Felix Vega[1, 4],
Lars Ole Fichte[3], Zouhair Nezhi[3], Chaouki Kasmi[1, 3], and Marcus Stiemer[3]**

Abstract—Uncertainty quantification and variability analysis are two domains of interest when looking at the efficiency of HPEM sources. Vircator is known to be a low efficiency high power microwave source subject to several generally volatile phenomena such as plasma expansion and shot-to-shot variability. In this study, a computationally low cost framework combining the Extreme Value Theory (EVT) and the Generalised Design of Experiments is proposed in order to study the peak power distribution of a Vircator obtained with a surrogate model. Following the pre-screening of random variables, the optimised parameters are introduced in 2.5D and 3D simulation tools, namely XOOPIC and CST-PS. It has been confirmed that the peak power output can reach a 40% increase. This shows that the EVT proves to be successful in classifying and quantifying random variables to influence the distribution tails.

1. INTRODUCTION

During the last decades, numerous statistical methods have been applied to electromagnetic [1–4] and mechanical problems [5] with the aim to quantify volatile effects. Applying a large spectrum of methods from central tendencies approaches [6, 7] to Extreme Value Theory (EVT) techniques [8], it has been shown how the confidence level of physical quantities can be assessed when dealing with random variables (RVs) [9]. Most studies in High Power Electromagnetics (HPEM) applications involving stochastic analysis focus on the general tendencies of physical quantities such as the ANOVA methodology which has been applied to Vircators in [10–13]. However, only a few studies were devoted to infer results on the distribution of extreme values, which would be a natural extension of the studies on central tendencies, mostly because of the difficulty to access experimentally the required data sets or due to the demanding computation power required to simulate complex and volatile systems. Assessing the probability of extreme values with high accuracy is of utmost importance for the characterisation of HPEM sources, especially with respect to source efficiency. Extreme Value (EV) statistics have been successfully applied to the study of electromagnetic waves coupling into cables and the conducted propagation in power networks [14]. To the authors' knowledge, no factor analysis quantifying their influence on EVs in the case of HPEM sources has been carried out so far.

Since high power devices are well known for their nonlinear behaviours, assuming random inputs naturally leads to an increase of the frequency of extreme values which eventually results in the maximisation of peak power. Nevertheless, this domain remains widely an open field of work due to the complexity to access a large data set necessary for studying extreme levels. The modelling and simulation of Vircators can be performed by means of different simulations tools such as XOOPIC [15] and CST-PS [16] which are 2.5D and 3D particle-in-cell simulations, respectively. Interestingly, recently,

a stochastic analysis of a Vircator, based on a surrogate model, has been proposed allowing the validation of the reliability of the system by studying RVs considering mechanical tolerances and pulsed power source variability [17]. Among many other advantages, the surrogate model allows for an efficient simulation at a reduced computational cost compared to XOOPIC and CST (surrogate: 19×10^{-6} s, CST-PS: 6.8×10^4 s, and XOOPIC: 7.9×10^2 s — results obtained for the same Vircator configuration and on the same computational platform) [17] enabling different statistical analysis. Applying sensitivity analysis techniques, such as Sobol and Morris indices, which only focus on general tendencies, it has been demonstrated that the anode-cathode gap has the highest influence on the power response, in the case of mechanical tolerances, while the charging voltage of the pulsed power source has the most significant influence as a volatile property of the electrical components. Moreover, the output peak power and radiated microwave signal frequency exhibit an interesting behaviour when being studied under the volatile influence of the RVs. One of the remaining key challenges is the maximisation of the peak power in a sense that is adapted to its volatile nature in order to improve the performance of a Vircator.

We propose, in this study, to analyse the tails of the stochastic distribution of the peak power that arises if certain system parameters are considered as RVs. While the resulting distribution of the peak power itself is too complex to be estimated, we profit from the Pickands-Balkema-de Haan theorem, which assures a Generalised Pareto Distribution (GPD) for the values exceeding a suitably chosen threshold independent of other properties of the distribution of the peak power. To avoid any bias, we chose this threshold to be the one-sided 95% quantile of the GPD. This threshold and the scale and shape parameters of the GPD identified for the excess values via a maximum likelihood method are used for the stochastic characterisation of power exceedances, and their dependence on the underlying RVs is analysed. Thus, the well-known formalism of very-high values over a threshold, developed to model *low probability - high consequence* events, is proposed. The influence of individual RVs on the distribution tails is analysed by studying the parameter importance of the RVs with respect to the arising threshold and the parameters of the identified GPD for the tail. For the input parameters providing a maximised peak power distribution, a numerically relatively costly validation of the proposed framework is computed with two simulation tools accurately considering the dynamics of particle oscillations between the anode and the emerging virtual cathode, which physically determines the properties of the Vircator. A schematic diagram showing the flow of the method proposed in this study is shown in Figure 1.

This paper is organised as follows. In Section 2, the surrogate model of the Vircator with the considered RVs is described. In addition, generalised Design of Experiments (DoE) is introduced as a
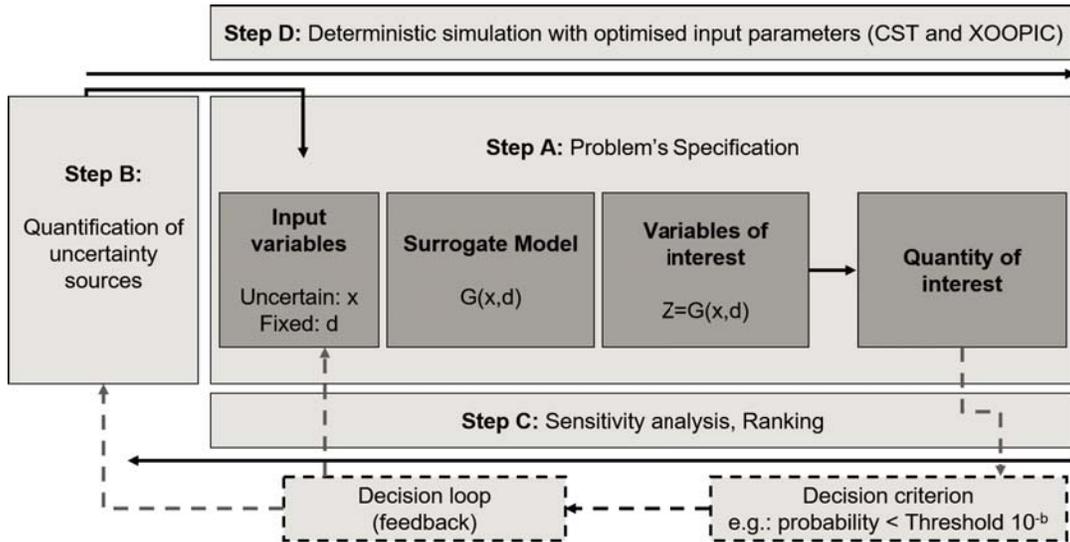

Figure 1. Uncertainties propagation and management framework.

method for factors analysis. In Section 3, the EVT is introduced along with the main statistical methods applied to identify the GPDs that characterise the asymptotic distribution of peak power exceedances. Relevant data are efficiently provided via Monte Carlo (MC) simulation. Section 4 is dedicated to variability analysis of the scale and shape parameters of the GPDs deduced thanks to the DoE process which provides an assessment of the influence of individual RVs on the EV statistics.

2. VIRCATOR SURROGATE MODEL, DOMAIN OF VALIDITY AND RANDOM VARIABLES

Recently, a surrogate model of the Vircator [18] has been proposed in order to perform stochastic simulations at reduced computational cost [17]. We describe in what follows the simulation framework and the related uncertain parameters considered in this study.

2.1. Vircator Surrogate Model

The HPEM source under study is the Axially Extracted Vircator (AEV) [19]. The physical operation of the Vircator [20–22] begins when the current injected in a vacuum drift-tube ($i_b(t)$) exceeds the space-charge-limiting current (I_{scl}). The surrogate model calculating the Vircator response, which was adopted in this paper, comprises two equations. The former one defines the dominant angular radiation frequency $\omega_{vc} = a_1\omega_p$ [23] with

$$\omega_p = \frac{2^{5/4}c}{3d}\sqrt{\frac{kVT_a}{\sqrt{kV+2}}},\tag{1}$$

and the second one calculates the power leaving the extraction surface at ω_p as [18]

$$\bar{P}_{\omega_p} = \frac{\pi^3 a_1^2 m}{12c^2 e}r_c^4\omega_p^4((kV+1)^2-1)^{3/2} \times e^{-4\left(1-\frac{8c^2((kV+1)^{2/3}-1)^{3/2}}{r_c^2\omega_p^2\left(1+\ln\left(\frac{r_{dt}}{r_c}\right)\right)\sqrt{(kV+1)^2-1}}\right)^2},\tag{2}$$

where c is the speed of light; m and e are the electron rest mass and charge; a_1 is a constant that could be approximated as 2.14 [22], and $k = e/mc^2$.

Equation (1) yields the relativistic plasma frequency [20] represented as a function of the Vircator design parameters. The domain of validity of the surrogate model, described by the combination of Eqs. (1) and (2), is studied and defined in [17, 23], showing applicability in a region of the variable space where particularly the optimal response of the Vircator is achieved. The particularity of this surrogate model is that it was adjusted to obtain lower error as the Vircator power limit was reached. Additionally, the model has been successfully used to optimise a previously constructed Vircator [24] and, recently, to predict the Vircator power limits [25].

Additionally, the model is a function of the mechanical and electrical design variables. Considering the mechanical inputs, the variables are the anode-cathode gap (d), anode transparency (T_a), cathode radius (r_c), and drift-tube radius (r_{dt}). On the electrical side, the only parameter is the anode cathode voltage (V). In a real application, the voltage is time varying ($V = v(t)$). In order to take into account the time dependency, we consider the coupling of the Vircator and a High Current Impulse Generator (HCIG) [26]. HCIG is a serial circuit formed by a capacitance (C_s) charged at $t = 0$ at V_0, an inductance (L_s), an internal source resistance (R_s), and the load impedance (R_l). The HCIG is a second order circuit that is connected to a nonlinear resistance given by Eq. (3). Consequently, the voltage (V) used to compute the output power in Eqs. (1) and (2) is time-varying, and the analytical solution of the differential equation for $v(t)$, which considers both the Vircator and the supplying network, cannot be solved in closed form. More details are presented in [17]. Because in a Vircator, the diode current is given by Child-Langmuir's law $i(t) = Kv(t)^{3/2}$ [27, 28], the diode (load) impedance can be defined as a function of the voltage or diode current as

$$R_l = \frac{v(t)}{i(t)} = \frac{1}{K^{2/3}i(t)^{1/3}},\tag{3}$$

where K is the diode perveance, and $i(t)$ is the circuit current. The perveance is a quantity that defines how significant the space charge effect is; its time-dependency is a consequence of the plasma

expansion [11]. The system efficiency is related to the coupling between the voltage source and the diode which therefore shows the importance of the perveance (linked to load impedance). The voltage waveform can be approximately obtained by numerical techniques if the plasma expansion is not considered. According to the Child-Langmuir's law, K is a function of d and r_c [29]. Interestingly, it has been observed that the simulation framework is capable of replicating the perveance variability due to plasma expansion and the shot-to-shot variability reported in the literature, as presented in [17].

2.2. Source of Uncertainties, Factors

Two kinds of random variables are introduced: the first set of RVs is related to the mechanical tolerances as defined in the ISO standard (ISO 2768-1:1989(en), General tolerances — Part 1: Tolerances for linear and angular dimensions without individual tolerance indications) (rows 1–4 in Table 1), and the second set of RVs describes the variability of the pulsed power source through the variation of electric components (rows 5–8 in Table 1). As already mentioned above, the pulsed power source is an RLC circuit comprising a capacitance C_s charged at V_0 at $t = 0$, an inductor L_s, and an internal resistance R_s. The load (Vircator diode) is connected using an ideal switch at $t = 0$ [17].

Using the parameters summarised in Table 1 as the central point of design, the estimated peak power is 305.9 MW, and the radiating frequency is 7.05 GHz.

Table 1. Definition of RVs.

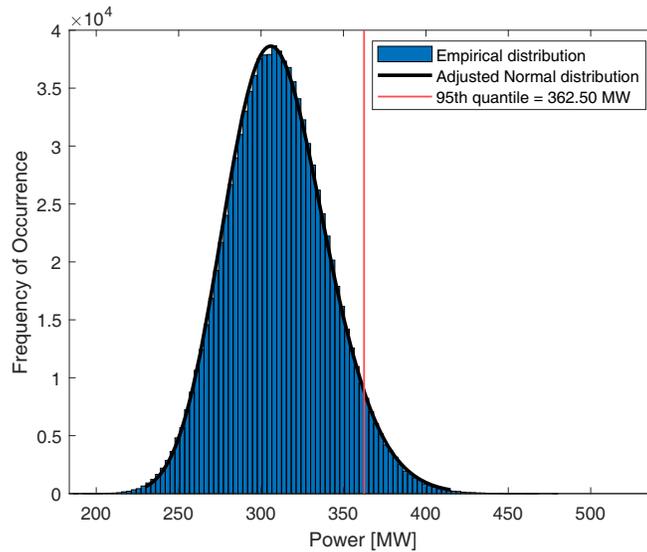| RV	PDF Type	PDF Mean	PDF CV (%)
d	Normal	8.1 [mm]	10
T_a	Normal	90 [%]	1
r_c	Normal	48 [mm]	1
r_{dt}	Normal	95 [mm]	1
V_0	Normal	1480 [kV]	10
L_s	Normal	0.2 [μH]	5
C_s	Normal	5 [nF]	10
R_s	Normal	3 [Ω]	10

Figure 2. Histogram of 1,000,000 Monte-Carlo computations of the output peak power considering the 8 RVs.

Running the MC simulation approach, Figure 2 shows an overview of the distribution of the peak power when considering the 8 RVs described in Table 1. The red mark stands for the 95% quantile level. Statistical central moments are a widely used method to study the variability of a physical quantity. The first statistical moment is the mean, and the second moment is the variance. These two moments measure what extent data are spread out about the average value of a distribution. Additionally, in descriptive statistics, the skewness and kurtosis, respectively the third and fourth statistical moments, are used to characterise the histogram form. The skewness allows for measuring the asymmetry of the probability density function of an RV around its mean value [30], whereas the kurtosis [30] is used to describe the shape of a distribution while focusing on the tails rather than on the peak. The higher the kurtosis is, the higher the extremity of outliers is.

A summary of the descriptive statistics is given in Table 2 [17]. To be able to decide whether the variation of a generally volatile variable has to be taken into account in a modelling approach or not, the sensitivity of the corresponding physical observable has to be determined. Here we propose to refer to the Generalised Design of Experiments summarised and applied in what follows. In addition to getting information about the sensitivity or importance of sets of volatile parameters, the DoE method gives us objective data that will show that extremal events (i.e., heavy tails) are indeed important for the resulting distribution of the peak power.

Table 2. Result of the random parametric variation for the Vircator under a non-ideal source [17].

| Parameter	Computed value
Mean	310.35 [MW]
Std	30.58 [MW]
Quantile 0.05	262.02 [MW]
Quantile 0.95	362.50 [MW]
Skewness	0.22
Kurtosis	3.07

The DoE is a statistical method that was implemented to allow the identification and quantification of the effects introduced by input random variables (so called factors) on the response of a system. In this study, the DoE technique is used to identify the way that the factors influence the Vircator's output peak power. Eight factors that possibly influence the Vircator's power response have been defined and listed in Table 1. Additionally, we are interested in studying the effects resulting from a variation of the factors both individually and as combinations in order to detect potentially correlated parameters. The considered combinations of RVs are represented in Table 7. To estimate the parameter sensitivity, we perform 256 sets of experiments covering all possible combinations of parameters (factors) defined either as random variables or fixed at their mean value (see column 3 in Table 1). The 256 sets consist of: 8 sets of experiments of 1st order where only one factor is varied, 28 sets of 2nd order where two parameters are varied at the same time, 56 sets of 3rd order with 3 factors varying at once, 70 sets of 4th order, 56 sets of 5th order, 28 sets of 6th order, 8 sets of 7th order, and one set of 8th order where all the parameters are varying.

To ease the readability, the following notation will be used: The value "0" implies that the factor was fixed at its mean value (see column 3, Table 1), and value "1" means that the factor was generated randomly with a normal distribution according to the percentage of variation defined in column 4, Table 1. The first experiment is the experiment with all factors remaining at their mean value, hence, being 0-th order (considered as the *design point* where no RVs are considered). Each set was numerated from the binary "00000000" (0) to "11111111" (255), as shown in Table 3, where each bit corresponds to the factors in the following order: $[d, T_a, r_c, r_{dt}, V_0, L_s, C_s, R_s]$.

For instance, Figure 3 shows the power output for the experiment "00100010" (34) where only r_c and C_s are considered as random variables. In Figure 3, it can be observed that the power increases with r_c and C_s and that the influence of the variability of C_s is more significant than that introduced by r_c.

Table 3. Generalised design of experiments — Combination of RVs.

Case	Order	d	T_a	r_c	r_{dt}	V_0	L_s	C_s	R_s
0	0	0	0	0	0	0	0	0	0
1	1	0	0	0	0	0	0	0	1
2	1	0	0	0	0	0	0	1	0
3	2	0	0	0	0	0	0	1	1
...									
254	7	1	1	1	1	1	1	1	0
255	8	1	1	1	1	1	1	1	1
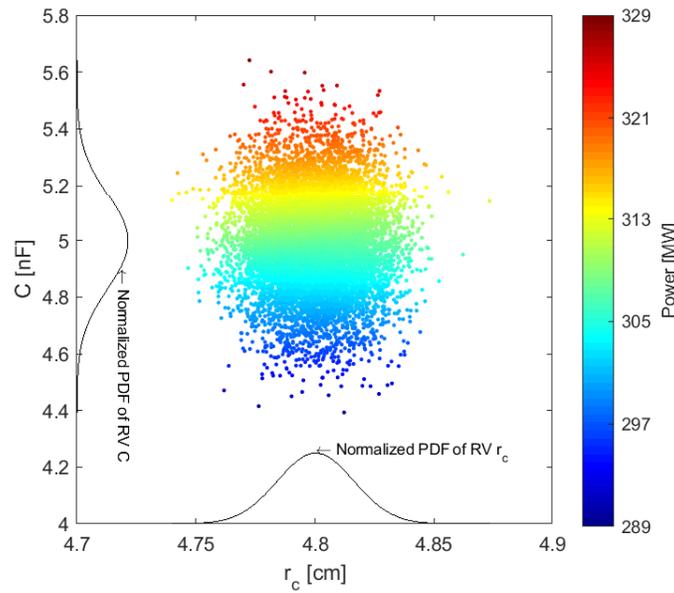
Figure 3. Monte-Carlo simulation — Computed peak power with r_c and C_s as RVs while d, T_a, r_{dt}, V_0, L_s, and R_s are fixed at their mean value.

This technique allows for studying all possible interactions between the factors and identifying the sets where the largest values of the peak power are reached. For each set 10,000 MC simulations have been performed in order to empirically ensure a sufficient number of random realisations. This was repeated four times, and a variation lower than 1% between the different samples was confirmed. As pointed out in [4], alternative sampling techniques could be useful to efficiently assess the quality of random simulations achieved for each set (e.g., bootstrapping, spectral techniques, etc.).

Interestingly, the effects of the RVs on the shape of the distribution can be observed by descriptive statistics. Moreover, when adjusting the PDF it has been shown that the Darlington Test only gives 75% success of inference that the output peak power distribution is likely to be a normal distribution. The test fails because of the discrepancy in adjusting the distribution tails as it can be observed in Figure 4. This is inferred since the kurtosis is close to 0 and the skewness close to 3 which are typical values of the normal distribution. It can be observed that the only discrepancy compared to a normal distribution is located in the tails. This is validated with the Quantile to Quantile (QQ) plot except for values below the 0.05 and above the 0.95 quantiles. This shows that extra care to distribution tails is required as the probability of having extreme values is relevant when looking at the increase of the peak output power. This is exactly the formal justification of a deeper study of the tails of the distribution of the radiated peak power as presented in the subsequent part of this work.
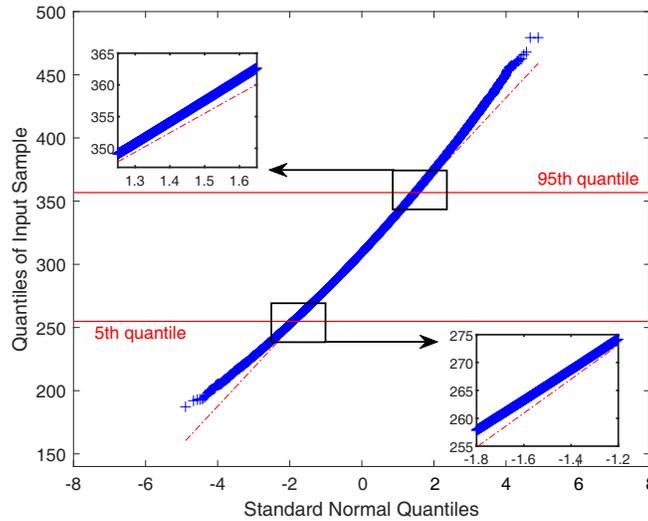
Figure 4. Quantile to quantile plot of the estimated power values against the theoretical quantile values of a standard normal distribution.

3. EXTREME VALUES THEORY (EVT)

Extreme value methods analyse the frequency of extreme variations from the mean of probability distributions. Two types of extreme value theorems allow for assessing the probability of extreme values: a first well-known approach deals with extracting the maxima over very large blocks. It is known that the maxima can be adjusted using the Generalised Extreme Value (GEV) distribution function family; a second method deals with finding the peak values that exceed a very high threshold, known as *Peaks Over Threshold* (POT) method. The probability distribution function of the peaks exceeding a certain threshold can be approximately fitted by a Generalised Pareto Distribution (GPD). The latter "universal property" of a large class of distributions with significant appearance of extremal events is a consequence of a theorem due to Pickands-Balkema-de Haan. In this study, we propose to focus on the second approach as it provides a well-established framework to analyse the exceedances over a very high threshold.

3.1. Probability Density Function (PDF)

The POT methodology involves the quantification of the probability distribution of the appearance of values over a certain threshold. Due to a theorem of Pickands-Balkema-de Haan [31], the cumulative density functions (CDFs) of these excesses converge with increasing threshold to the CDF of a GPD, which is defined by:

$$F_{\sigma,k}(x) = \begin{cases} 1 - \left(1 + \dfrac{k}{\sigma}x\right)^{-\frac{1}{k}}, & k \neq 0 \\ 1 - \exp\left(-\dfrac{x}{\sigma}\right), & k = 0 \end{cases} \tag{4}$$

where k and σ are the shape and scale parameters, respectively (see examples in Figure 5 and Figure 6).

Interestingly, the values of the shape parameter can be used to classify the distribution function as either: fat-tailed, thin-tailed, or short-tailed. In other words, the function becomes a usual Pareto function when $k > 0$, exponential distribution for $k = 0$, or a Type-II distribution for $k < 0$ (note that it becomes a uniform distribution for $k = -1$). The scale parameter $\sigma > 0$ describes the expected amount of variation in the output. When $\sigma > 1$, the distribution stretches, and when $\sigma < 1$, it compresses. Moreover, a scale parameter of 1 causes no changes in the distribution. For short, the larger the scale is, the more spread out the distribution is.
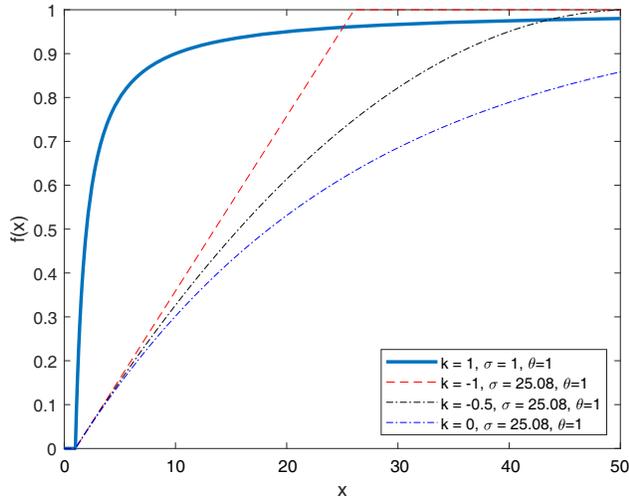
Figure 5. Three cumulative distribution functions for different shape parameters of the GPD with a fixed scale value.
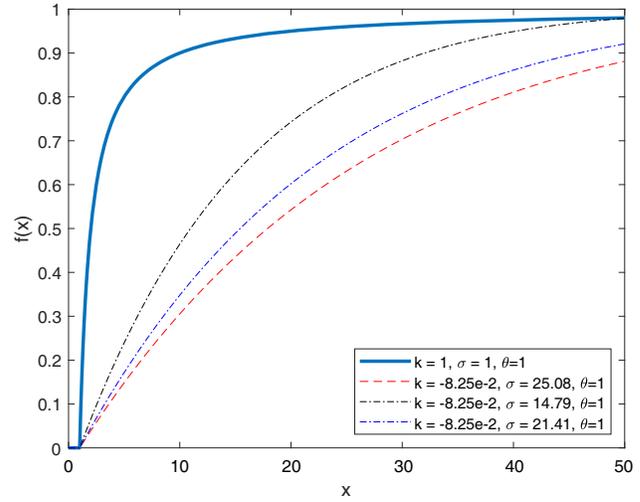
Figure 6. Three cumulative distribution functions for different scale parameters of the GPD and a fixed shape value.

3.2. Estimation of the Threshold

Threshold selection is a critical step in order to obtain accurate model parameters. A number of threshold selection methods can be found in the literature, such as Scarrott and MacDonald [32], Caeiro and Gomes [33] which comprise the mean residual life plot and threshold stability plot. However, these classes of graphically based methods often lack an objective criterion to conclude the threshold without any human bias from the data and are particularly not suited for automated identification processes. Relying on the analysis of the statistics of extreme tendencies, the quantile method was chosen for being a sufficient and efficient straightforward estimator. In this study, the values are considered extreme if their level is above the one-sided 95% quantile [32].

3.3. Distribution Parameters

The parameters of the generalised Pareto distribution have been computed using the maximum log-likelihood equation [34] as no direct solution exists to estimate the GPD parameters:

$$l(\sigma, k) = -n \log \sigma - \sum_{i=1}^{n} \frac{k+1}{k} \log \left(1 + \frac{kx_i}{\sigma} \right) \tag{5}$$

where x_i is the sample under study of n values. Equation (5) represents the term for $k \neq 0$, which is continued to $k = 0$ by the logarithm of the derivative of the corresponding term in Equation (4). Thus, a numerical algorithm has been implemented to determine σ and k such that Equation (5) is maximised for the given set of peak powers x_i exceeding the threshold given by the 95% quantile.

3.4. Importance of the 8 RVs for the GPD Parameters for the Output Peak Power

As mentioned previously, based on a Monte Carlo (MC) simulation, the surrogate model of the Vircator has been used to generate 1,000,000 random configurations. This was repeated for 100 sets to ensure the convergence of the GPD parameters fitted to the data sets. A graphical validation of the selection of the threshold can also be obtained by using the QQ plot. The QQ plot was computed for the 1,000,000 MC random configurations considering the 8 RVs as shown in Figure 4 showing a good agreement between the quantile approach and the graphical technique. The GPD was fitted on values higher than the 95% quantile (362.50 MW). The computed shape and scale parameters are −0.0985 and 16.0974 MW, respectively. The resulting inferred GPD and the empirical distribution are depicted in Figure 7. It can
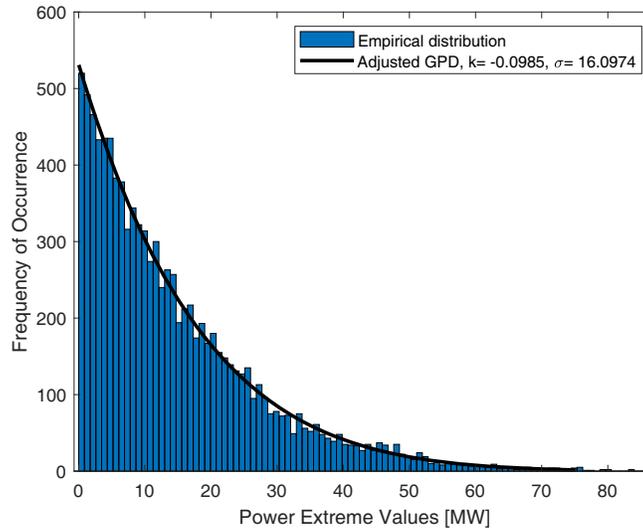
Figure 7. Histogram of the peak power extreme values considering the 8 RVs and the inferred GPD.

be observed that a very good fit of the extreme values is obtained highlighting the applicability of the *peaks over a threshold* approach to model the distribution tails.

4. FACTOR ANALYSIS APPLIED TO EXTREME VALUES

In the previous section, the applicability of the POT approach to study the extreme values of the output peak power based on the surrogate model of the Vircator has been shown. We propose in what follows to study the influence of RVs on the adjusted GPD considering all possible RVs combinations.

4.1. Variability of the Threshold, Scale and Shape

The use of the 95% quantile, later called threshold, is well-accepted and therefore computed for each of the 256 sets of experiments with the help of 10,000 simulations (it has been found that the convergence of the 4 first statistical moments and the thresholds is obtained with less than 1% of variation for the 256 configurations). Estimated thresholds are depicted in Figures 9(b)–(c).

In Figure 8, it can be noticed that the values are divided into three distinct groups: around 300 MW, 320 MW, and 360 MW. The mean value of the estimated thresholds for the 256 configurations was found to be 340.63 MW. Analysing the data, it is concluded that all values greater than 350 MW are obtained when considering the voltage V_0 as a RV. The maxima of thresholds for each order of combination are given in Table 4. The highest threshold was 362.96 MW which corresponds to the 6th order of RVs combination, with the variables T_a and r_c being the ones assumed at their mean levels, while the rest are RVs defined in Table 1. It is noted that the same combination set can reach a maximum power as high as 443.26 MW.

The scale (σ) and shape (k) parameters were found for each combination. The scale parameter shows the stretching or shrinking of the tail. In other words, the larger the scale parameter is, the more spread out the distribution is, whereas the shape parameter shows the tail index. The scale (σ) and shape (k) parameters are plotted in Figures 9(a)–(c) for the selected threshold and power output. Also, the maxima of scale parameters for each order of combination are given in Table 5. The shape parameter is considered dominant in finding the qualitative behaviour of the GPD. In our case, negative k shows that the distribution of the outliers has a mean upper bound of 404.35 MW. The maximum upper bound computed was 426.68 MW which corresponds to the combination of 6 RVs where T_a and r_c are fixed (see Figure 17, at the end of the paper).

Figure 9 gives an overview of the distributions of shape (k) and scale (σ) values. On the one hand, the σ-parameter seems of utmost importance since two sets of populations can be seen from
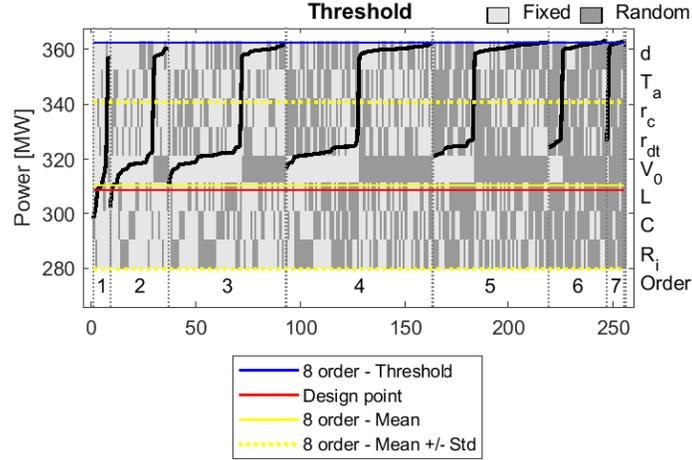
Figure 8. Computed threshold parameter for each set of the 256 possible combinations as a result of the RVs (vertical scale stands for the RVs combination). The sets have been grouped by order and sorted from lower to higher values.

Table 4. Maxima of thresholds for each order with related combination of RVs.

Order	d	T_a	r_c	r_{dt}	V_0	L_s	C_s	R_s	Thresholds [MW]
1	0	0	0	0	1	0	0	0	356.9
2	0	0	0	0	1	1	0	0	360.4
3	1	0	0	0	1	1	0	0	361.6
4	1	0	0	0	1	1	1	0	362.1
5	1	0	1	0	1	0	1	1	362.4
6	1	0	0	1	1	1	1	1	362.9
7	1	0	1	1	1	1	1	1	362.7
8	1	1	1	1	1	1	1	1	362.5

Table 5. Maxima of scale values [MW] per orders with related combinations of RVs.

Order	d	T_a	r_c	r_{dt}	V_0	L_s	C_s	R_s	Scale
1	0	0	0	0	1	0	0	0	15.77
2	1	0	0	0	1	0	0	0	16.34
3	1	0	0	0	1	1	0	0	16.18
4	0	0	1	0	1	1	1	0	18.02
5	0	1	1	0	1	1	1	0	18.29
6	1	0	1	0	1	1	1	1	19.44
7	1	1	1	1	1	1	1	0	17.68
8	1	1	1	1	1	1	1	1	16.09

Figure 9: the first around 3 and the second around 16. On the other hand, the k-parameter provides only one characteristic region (around -0.15). Figure 11 further emphasises the importance of the voltage parameter V_0 in maximising the output peak power. This is because all scale parameters above 13.65 MW belong to a combination of RVs where V_0 is involved. Even though the significance of the voltage parameter V_0 is notable, increasing V_0 does not always result in increasing the power. Based on
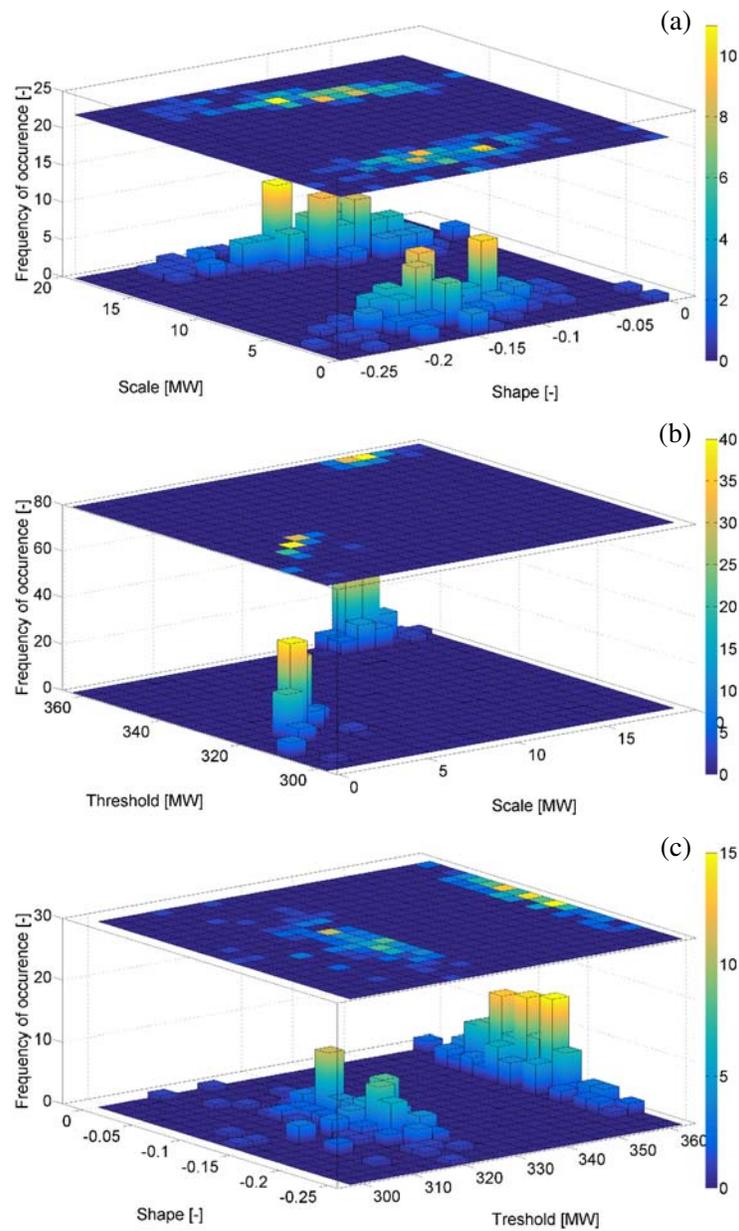
Figure 9. Bivariate histograms of the pairs of parameters. (a) Shape and scale. (b) Scale and threshold. (c) Threshold and shape.

the observations published by Neira et al. [18] (see Figure 2), it can be concluded that the significance of the voltage (as a RV) depends on the central point of design. Thus, for a given setup, the power can increase or decrease, and also the grade of importance can change, therefore, highlighting the importance of the obtained results. Furthermore, the maximum scale parameter computed was 19.45 Mw which is corresponding to the following combination of RVs where T_a and r_{dt} are fixed at their mean values.

Figure 10 strengthens previous remarks (see data in Figure 9) considering the relative minor influence of the shape parameter k. Indeed, the results given in Figure 10 provide a global overview of the shape parameter previously extracted with respect to the different sets of data involving respectively 1, 2, ..., 7 RVs (so-called 1st, 2nd, ..., 7th RV order). In Figure 10, the results are sorted: first considering the different RV orders, then, ordering each set of inputs from lower to higher shape parameter (black plain line).
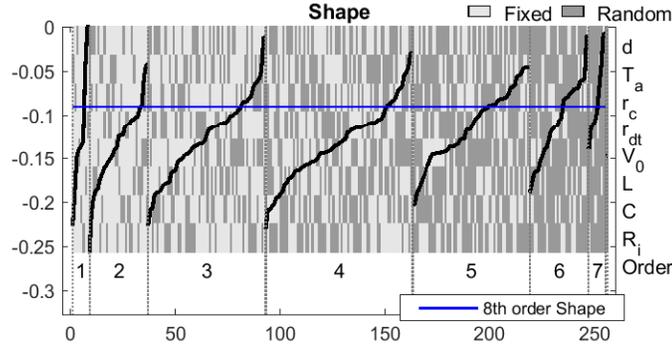
Figure 10. Computed shape parameter for each set of the 256 possible combinations as a result of the RVs (vertical scale stands for the RVs combination). Shape parameter values have been sorted from lower to higher values within each combination orders 1–7.

The random nature of a given input is indicated by a darker colour from the grey scale, whereas the fixed parameters (i.e., parameters given from its initial deterministic value) are represented by light grey colour. The results for the 8th RV order, where all variables are varied, are given as a reference displayed by a plain blue line.

As previously underlined (see Figures 5 and 6), the variation of the scale parameter around its mean value seems larger than that of the shape parameter. The results given in Figure 10 reinforce this conclusion since none of the sets of input combinations (here with orders 1, 2, ..., 7) seems to play a major role compared to other sets. The results in Figure 11 dealing with scale parameter and threshold paint a completely different picture from the latest conclusions about the shape parameter. Thus, the figures clearly lay emphasis on the importance of the V_0-parameter. Assume that V_0 as a random or deterministic parameter (respectively dark or light grey colouring) obviously involves huge gaps respectively considering threshold power (see the black plain line above) and the scale parameter (see the black plain line below).
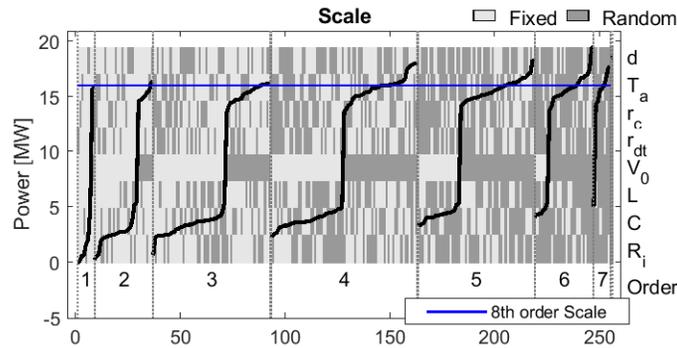

Figure 11. Computed scale parameter for each set of the 256 possible combinations as a result of the RVs (vertical scale stands for the RVs combination). The sets have been grouped by order and sorted from lower to higher values.

Firstly, the results in Figures 12–18(a) clearly exhibit the overwhelming impact of the V_0-parameter, when dealing with threshold power (and considering each of the classes defined by the DoE of 1st, 2nd, ..., 7th RV order):

- each of the aforementioned figures shows huge power gaps when V_0 is considered as a random variable (see rows "V_0" in Figures 12–18);
- considering the power results closer to the "8th order threshold" (blue plain line) in Figures 17 and 18, the importance of the anode-cathode gap d is also demonstrated on the same figures (which
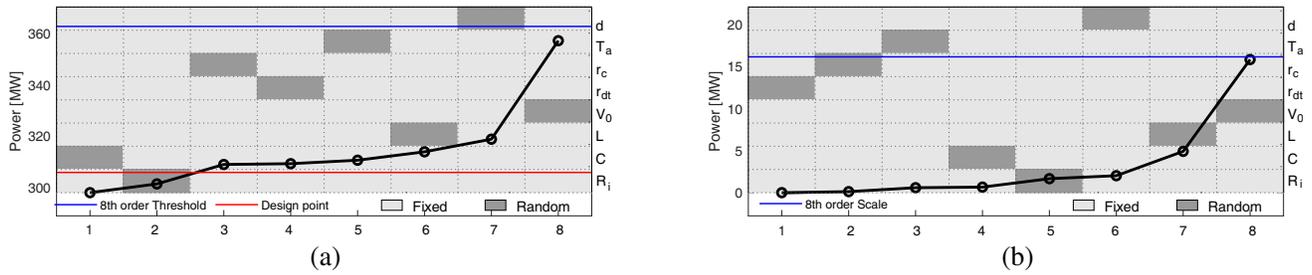
Figure 12. (a) Sorted threshold and (b) scale values obtained for 1 RV.
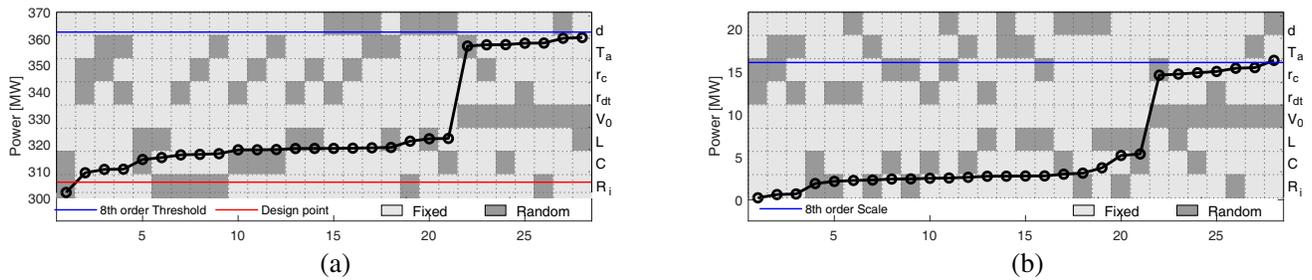

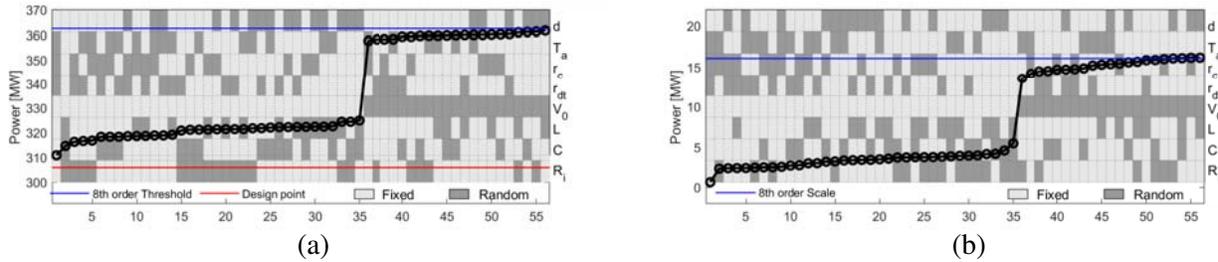**Figure 13.** (a) Sorted threshold and (b) scale values obtained for 2 RVs.

Figure 14. (a) Sorted threshold and (b) scale values obtained for 3 RVs.
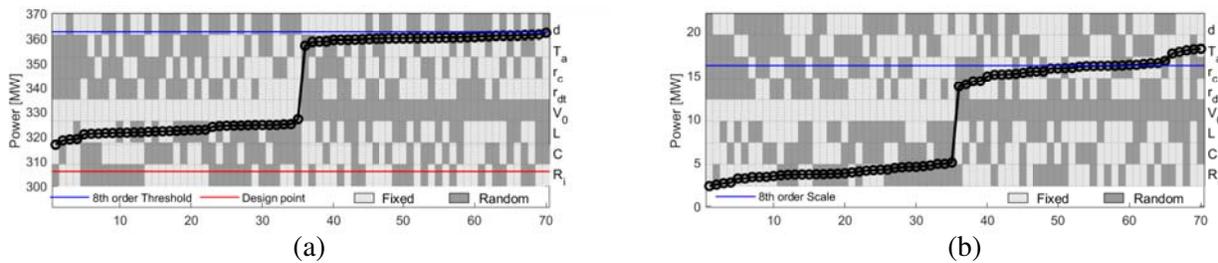

Figure 15. (a) Sorted threshold and (b) scale values obtained for 4 RVs.

is also well known for its influential role when dealing with Vircator peak power generation);

- as a reminder, it has been previously underlined that the higher threshold was obtained assuming T_a and r_c as deterministic parameters (i.e., considering the two inputs as least influential ones, see Figure 17).

Similar to the previous discussion, the most influential parameters inferred from sorted scale values can be ranked from Figures 12–18(b):
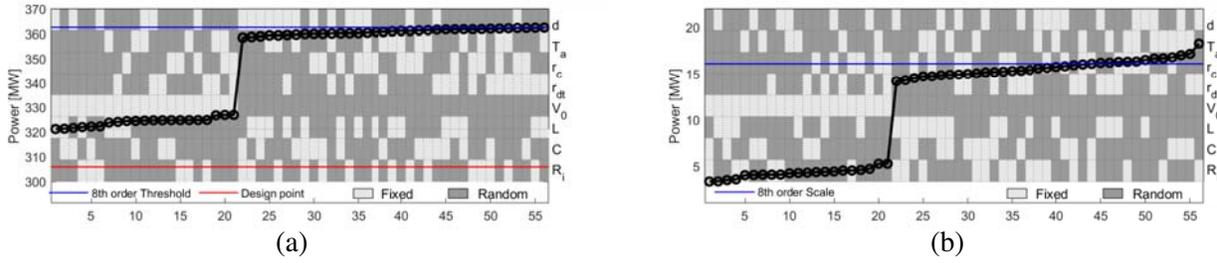
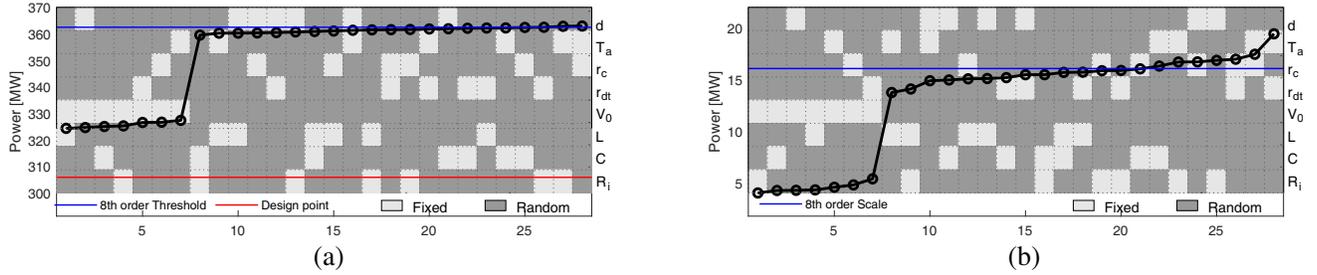**Figure 16.** (a) Sorted threshold and (b) scale values obtained for 5 RVs.

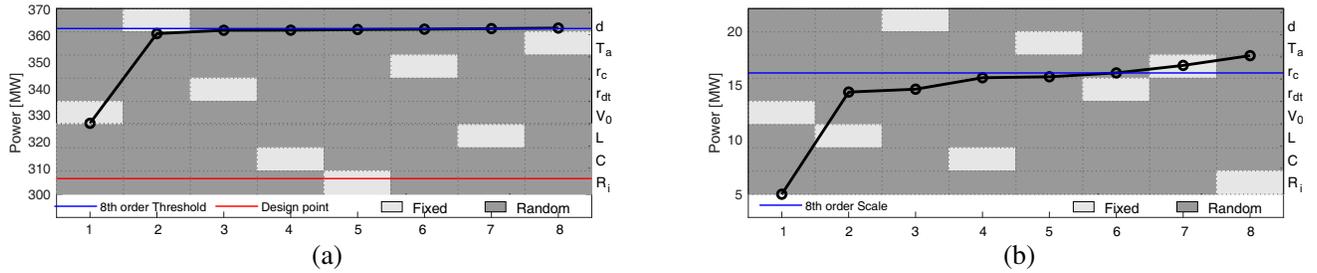**Figure 17.** (a) Sorted threshold and (b) scale values obtained for 6 RVs.

Figure 18. (a) Sorted threshold and (b) scale values obtained for 7 RVs.

- V_0 seems also to play a major role since its random assumption involves getting closer to the expected results for 8 RVs (reference plain blue line);
- the effect of the d-parameter should be taken into consideration (e.g., see Figure 18 when dealing with 7 RVs), but the inductance L_s is also carefully considered;
- on the opposite, the parameters T_a, r_c, and r_{dt} seem least influential as depicted in Figures 12–18.

4.2. RVs Reduction and Maximisation of the Peak Power

In the previous section, it has been shown that specific RVs and their combinations have a non-negligible influence on the peak power statistics. Hereafter, the aim is to increase the probability of events with a high peak power value as well as the height of that value at the same time. The resulting configurations are selected based on a multi-objective optimisation (i.e., Pareto optimisation) of the scale and threshold parameters obtained from the GPD through the following conditions:

- Increase of the location (threshold) and heaviness of the distribution tails (scale): configurations of RVs are selected when the estimated threshold is above the central point of design, and the scale exceeds the value obtained when considering the 8 RVs.

- Complexity reduction: configurations of RVs are selected when both GPD parameters are above the values obtained for the 8 RVs configurations. This condition is proposed in order to reduce the number of RVs which would require extra precaution during the design process.

Table 6. Detected configurations giving thresholds and scale parameters above the design point values and above the values computed for the 8 RVs.

Parameter	Configurations
Threshold	159, 190, 191
Scale	14, 15, 31, 46, 47, 60, 61, 78, 89, 91, 92, 95, 105, 107, 110, 120, 126, 136, 137, 140, 141, 153, 154, 156, 157, 158, 159, 168, 169, 170, 171, 173, 174, 175, 189, 190, 203, 207, 220, 221, 223, 232, 239, 254
Common Configurations	159 (Order 6) 190 (Order 6)

Table 7. Combination of RVs maximising the threshold and the scale.

Case	Order	d	T_a	r_c	r_{dt}	V_0	L_s	C_s	R_s
159	6	1	0	**0**	1	1	1	1	**1**
190	6	1	0	**1**	1	1	1	1	**0**

Table 6 presents the configurations where the threshold and scale parameters exceed the value computed by the 8 RVs configuration. Additionally, the common configurations where both threshold and scale parameters were surpassed are extracted and presented in Table 6 as well. Table 7 shows a binary description of common cases where 1 means that the variable was driven as an RV whereas 0 means that the variable was fixed at its mean value (see Table 1). Interestingly the two remaining combinations have the following particularity:

- Order of remaining configurations is 6 for both.
- Anode transparency is not considered as an RV and fixed at its mean value.
- r_c and R_s are in opposite considerations: in case 159, r_c is fixed at its mean value and R_s considered as a RV and for case 190, and r_c is considered as a RV and R_s fixed at its mean value.
- All other parameters are considered as RVs

Using the input values which yield the extreme values of the two sets 159 and 190, the radiated frequency is also statistically assessed in order to evaluate the influence of the listed maximisation on the radiation frequency of the Vircator. The mean and the standard deviation of the radiation frequency for the input parameters configurations resulting in extreme values are proposed in Table 8. The design point gives a frequency of 7.05 GHz. This shows that the resulting maximised peak power is obtained at a frequency in a given statistical interval (mean $+/-$ standard deviation).

4.3. Deterministic Solution with Optimised Input Parameters

In the previous sections, the pre-optimisation of the Vircator's peak power based on EVT and the surrogate model were presented. This initial process allows for identifying the parameters that resulted in the maximisation of the peak power, which belonged to the 159 and 190 configurations. CST-PS and Xoopic simulation softwares are used in order to confirm the increase of the peak power output using the pre-screened parameters.

Table 8. The corresponding distribution parameters, variability of the radiated frequency, and perveance resulting from the configurations of the RVs maximising the peak power.

Case	Threshold [MW]	Scale [MW]	Shape	95% quantile	Frequency [GHz] mean; std	Perveance $[\mu AV^{-3/2}]$
159	362.86	17.47	-0.14	404.85	7.20; 0.171	258.2
190	362.95	16.72	-0.10	404.80	7.19; 0.166	251.9
255	362.50	16.05	-0.09	403.70	7.18; 0.167	257.9

The XOOPIC simulation of the Vircator is shown in Figure 19(a). The setup of the simulation was performed using 40 cells in $\hat{x}$ and 40 in $\hat{r}$. The total simulation time was 100 ns. The CST model, shown in Figure 19(b), was simulated using Explosive Electron Emission with a rise time of 0.5 ns, a threshold field of 25 kV/m, and 924 emission points over the cathode surface.

The Vircator's power output is estimated according to [35] as follows: the area of the extraction window (A_w) is divided in $n = 40$ and $n = 96$ parts of area A_i for XOOPIC and CST-PS, respectively. Time-domain Magnetic $(H_i(t))$ and Electric $(E_i(t))$ probes were placed in the centre of each subdivision. Subsequently, Fast Fourier Transform (FFT) was applied to the signal recorded by each probe. Then, the Poynting Vector is obtained with $S_i(f) = E_i(f) \times H_i(f)^*$, where * denotes the complex conjugate operator. Finally, the output peak power P is obtained with $\sum_{i=1}^{n} S_i(f) \cdot A_i$.

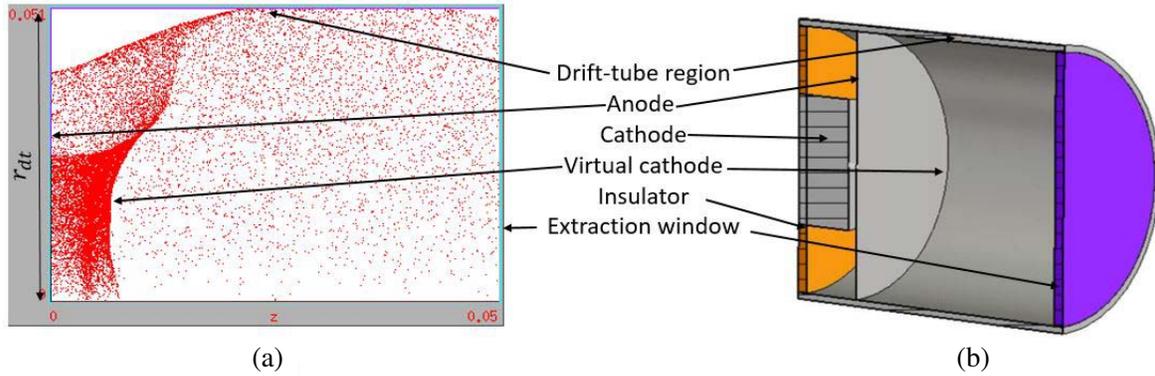(a)   (b)

Figure 19. Vircator model simulated using (a) XOOPIC and (b) CST-PS.

Table 9. Estimated peak power and the corresponding radiation frequency obtained from the surrogate model, XOOPIC and CST results for the two RVs configurations maximising the peak power (159 and 190) and the point of design (0).

Config.	Simulation tool	Peak Power [MW]	Frequency [GHz]
	XOOPIC	330	6.83
0	CST-PS	273	6.90
	Model	305	7.05
	XOOPIC	469	7.15
159	CST-PS	408	6.33
	Model	444	7.47
	XOOPIC	482	7.15
190	CST-PS	419	6.3
	Model	435	7.3

The results are summarised in Table 9. The values found for the peak power obtained by CST-PS, Xoopic, and the surrogate model are in good agreement (0.44 dB maximum difference between CST-PS and XOOPIC with the surrogate model). However, for the dominant frequency, CST simulations present high deviation from the value determined by the surrogate model and the frequency obtained in XOOPIC. This level of differences has also been reported by several authors, e.g., see in [35, 36], and requires further investigations.

Results summarised in Table 9 demonstrate that statistically, the Vircator peak power output can reach higher levels if special attention is given to the design and manufacturing of the Vircator and the pulsed power source.

5. CONCLUSIONS

In this paper, eight parameters have been considered as possibly volatile design parameters in the analysis of the surrogate model of a Vircator. Introducing them as RVs into the model allows to consider mechanical tolerances and power electronic variabilities. The extreme value theory has been introduced in order to be able to determine the statistical distribution of extreme peak power values. The extreme value statistics based on the *peaks over a threshold* approach was applied in order to analyse and estimate the PDFs of the extreme values considering the 95% quantile as threshold. The required empirical data on peaks exceeding a very high threshold to identify the scale and the shape parameter of the Generalised Pareto Distribution sets of up to 8 RVs have been provided by MC simulations. It has been shown that the theoretically granted convergence of the distribution of extremal events to a Generalised Pareto Distribution leads in the given situation to a sufficiently accurate fit of the generalised Pareto Distribution to the data obtained by the MC simulation.

In order to understand the influence of RVs on the peak power statistics, the generalised design of experiments has been combined with the extreme value statistics. Applying the design of experiments, 256 sets of experiments were generated consisting of all possible combinations of RVs. Generally, the design of experiments is applied in order to assess the influence of RVs (also called factors) on the general tendencies. In this study, the focus has been laid on the variability of Generalised Pareto Distribution parameters, i.e., scale and shape parameters, and on the influence on the threshold.

Analysing the influence of RVs on the different parameters, it has been observed that the shape parameter has a low variability showing that the Generalised Pareto distribution is likely to be in the form of the exponential distribution (shape $= 0$). Regarding the threshold and scale, the configurations giving the highest values have been selected in order to extract the combination of RVs giving the highest extreme values for a given quantile. It has been deduced that two combinations of six RVs allow for maximising statistically the peak power. Two parameters, namely r_c and R_s, exhibit an interesting behaviour: they both require an opposite consideration where one of them is considered an RV and the other one fixed at its mean value. 30% higher peak power output could be obtained with a relatively small frequency shift compared to the point of design.

Future work will be dedicated to the optimisation of input variables with a focus on the peak output power extreme values when fixing the frequency. The authors expectation is that this will introduce a new constraint on the nominal point of design related to the frequency variability. Developing an efficient source at a given frequency with defined acceptable boundaries tailored for a specific application will be further investigated.

REFERENCES

1. Wang, Y. and W. Xu, "Probability statistical method of assisting electromagnetic compatibility index decision-making," *2018 IEEE International Symposium on Electromagnetic Compatibility and 2018 IEEE Asia-Pacific Symposium on Electromagnetic Compatibility (EMC/APEMC)*, 509–512, May 2018.
2. Zhao, Y., X. Zhao, L. Yan, H. Zhou, and K. Huang, "High frequency response sensitivity of electrically large enclosure with aperture and its statistical analysis method," *2015 Asia-Pacific Symposium on Electromagnetic Compatibility (APEMC)*, 185–188, May 2015.

3. Liang, T., G. Spadacini, F. Grassi, and S. A. Pignari, "Coupling of wideband radiated IEMI to wiring harness: A statistical analysis of the main in uencing parameters," *2018 IEEE Symposium on Electromagnetic Compatibility, Signal Integrity and Power Integrity (EMC, SIPI)*, 357–362, July 2018.

4. Lallechere, S., C. Carobbi, and L. Arnaut, "Review of uncertainty quantification of measurement and computational modeling in EMC — Part II: Computational uncertainty," *IEEE Transactions on Electromagnetic Compatibility*, Vol. 61, No. 6, 1699–1706, December 2019.

5. Saleem, I., M. Aslam, and M. Azam, "The use of statistical methods in mechanical engineering," *Research Journal of Applied Sciences Engineering and Technology*, Vol. 5, 2327–2331, March 2013.

6. Yin, H., J. Lan, and X. R. Li, "New robust metrics of central tendency for estimation performance evaluation," *2012 15th International Conference on Information Fusion*, 2020–2027, 2012.

7. Tahir, M. M., A. Q. Khan, N. Iqbal, A. Hussain, and S. Badshah, "Enhancing fault classification accuracy of ball bearing using central tendency based time domain features," *IEEE Access*, Vol. 5, 72–83, 2017.

8. Nourshamsi, N., J. C. West, C. E. Hager, and C. F. Bunting, "Generalized extreme value distributions of fields in nested electromagnetic cavities," *IEEE Transactions on Electromagnetic Compatibility*, Vol. 61, No. 4, 1337–1344, 2019.

9. Houret, T., P. Besnier, S. Vauchamp, and P. Pouliguen, "Estimating the probability density function of the electromagnetic susceptibility from a small sample of equipment," *Progress In Electromagnetics Research B*, Vol. 83, 93–109, 2019.

10. Roy, A., R. Menon, S. K. Singh, M. R. Kulkarni, P. C. Saroj, K. V. Nagesh, K. C. Mittal, and D. P. Chakravarthy, "Shot to shot variation in perveance of the explosive emission electron beam diode," *Physics of Plasmas*, Vol. 16, No. 3, 033113, 2009. [Online]. Available: https://doi.org/10.1063/1.3097903.

11. Roy, A., R. Menon, K. V. Nagesh, and D. P. Chakravarthy, "High-current density electron beam generation from a polymer velvet cathode," *Journal of Physics D: Applied Physics*, Vol. 43, No. 36, 365202, August 2010.

12. Roy, A., S. K. Singh, R. Menon, D. Senthil Kumar, S. Khandekar, V. Bhaskar Somu, S. Chottray, P. C. Saroj, K. V. Nagesh, K. C. Mittal, and D. P. Chakravarthy, "Pulsewidth variation of an axial vircator," *IEEE Transactions on Plasma Science*, Vol. 38, No. 7, 1538–1545, 2010.

13. Roy, A., A. Sharma, V. Sharma, A. Patel, and D. P. Chakravarthy, "Frequency variation of a re ex-triode virtual cathode oscillator," *IEEE Transactions on Plasma Science*, Vol. 41, No. 1, 238–242, 2013.

14. Kasmi, C., M. Hélier, M. Darces, and E. Prouff, "Generalised pareto distribution for extreme value modelling in electromagnetic compatibility," *Electronics Letters*, Vol. 49, No. 5, 334–335, 2013.

15. Verboncoeur, J. P., M. V. Alves, V. Vahedi, and C. K. Birdsall, "Simultaneous potential and circuital solution for 1D bounded plasma particle simulation codes," *Computational Physics*, Vol. 104, No. 2, 321–328, 1993.

16. CST, CST STUDIO SUITE, Charged Particle Simulation, CST — Computer Simulation Technology, 2019.

17. Almansoori, M., E. Neira, S. Lallechere, C. Kasmi, F. Vega, and F. Alyafei, "Assessing vircators' reliability through uncertainty and sensitivity analyses using a surrogate model," *IEEE Access*, Vol. 8, 205 022–205 033, 2020.

18. Neira, E., Y.-Z. Xie, and F. Vega, "On the virtual cathode oscillator's energy optimization," *AIP Advances*, Vol. 8, No. 12, 125210, 2018. [Online]. Available: https://doi.org/10.1063/1.5045587.

19. Choi, M. C., S. H. Choi, M. W. Jung, K. K. Seo, Y. H. Seo, K. S. Cho, E. H. Choi, and H. S. Uhm, "Characteristic of vircator output at various A-K gap distances with diode perveance," *IEEE Conference Record — Abstracts. PPPS — 2001 Pulsed Power Plasma Science 2001. 28th IEEE International Conference on Plasma Science and 13th IEEE International Pulsed Power Conference (Cat. No.01CH37)*, 503, June 2001.

20. Benford, J., J. Swegle, and E. Schamiloglu, *High Power Microwaves (Ser. Series in Plasma Physics)*, CRC Press, 2007. [Online]. Available: https://books.google.ae/books?id= qHCPPQvr12sC.

21. Petren, J., "Frequency tunability of axial cavity vircators and double anode vircators," Master's thesis, School of Electrical Engineering (EES), KTH, 2016.

22. Alyokhin, B. V., A. E. Dubinov, V. D. Selemir, O. A. Shamro, K. V. Shibalko, N. V. Stepanov, and V. E. Vatrunin, "Theoretical and experimental studies of virtual cathode microwave devices," *IEEE Transactions on Plasma Science*, Vol. 22, No. 5, 945–959, October 1994.

23. Neira, E., "Study on the optimization of virtual cathode oscillators for high power microwaves testing," Ph.D. dissertation, Universidad Nacional de Colombia, Bogota, Colombia, September 2019.

24. Neira, E. and F. Vega, "On the use of xoopic for the simulation of virtual cathode oscillators," *European Electromagnetics Symposium 2016*, August 2016.

25. Neira, E., F. Vega, C. Kasmi, and F. AlYafei, "On the power limits of an axially extracted virtual cathode oscillator," *IEEE Transactions on Plasma Science*, Vol. 48, No. 11, 3822–3826, 2020.

26. Kuffel, E., W. Zaengl, and J. Kuffel, *High Voltage Engineering Fundamentals*, 2nd Edition, 1–7, Newnes, Oxford, 2000. [Online]. Available: http://www.sciencedirect.com/science/article/pii/B9780750636346500022.

27. Child, C. D., "Discharge from hot cao," *Phys. Rev. (Series I)*, Vol. 32, 492–511, May 1911. [Online]. Available: http://link.aps.org/doi/10.1103/PhysRevSeriesI.32.492.

28. Langmuir, I., "The effect of space charge and residual gases on thermionic currents in high vacuum," *Phys. Rev.*, Vol. 2, 450–486, December 1913. [Online]. Available: http://link.aps.org/doi/10.1103/PhysRev.2.450.

29. Choi, E. H., M. C. Choi, S. H. Choi, K. B. Song, Y. Jung, Y. H. Seo, H. M. Shin, H. S. Uhm, D. W. Lim, C. H. Kim, J. M. Lee, and J. W. Ahn, "Characteristics of diode perveance and vircator output under various anode-cathode gap distances," *IEEE Transactions on Plasma Science*, Vol. 30, No. 5, 1728–1732, 2002.

30. Kim, H.-Y., "Statistical notes for clinical researchers: Assessing normal distribution (2) using skewness and kurtosis," *Restorative Dentistry Endodontics*, Vol. 38, 52–54, February 2013.

31. Balkema, A. A. and L. de Haan, "Residual life time at great age," *Ann. Probab.*, Vol. 2, No. 5, 792–804, October 1974. [Online]. Available: https://doi.org/10.1214/aop/1176996548.

32. Scarrott, C. and A. MacDonald, "A review of extreme value threshold estimation and uncertainty quantification," *Revstat Statistical Journal*, Vol. 10, 33–60, March 2012.

33. Caeiro, F. and M. Gomes, *Threshold Selection in Extreme Value Analysis: Methods and Applications*, 69–86, Chapman and Hall, December 2015.

34. Tajvidi, N., "Characterisation and some statistical aspects of univariate and multivariate generalised pareto distributions," Chalmers University Of Technology, September 1999.

35. Clements, K. R., R. D. Curry, R. Druce, W. Carter, M. Kovac, J. Benford, and K. McDonald, "Design and operation of a dual vircator HPM source," *IEEE Transactions on Dielectrics and Electrical Insulation*, Vol. 20, No. 4, 1085–1092, 2013.

36. Han, S. H., J. S. Choi, S. H. Baek, and T. Hurtig, "Particle simulation of coaxial vircator," *ASIAEM 2015, Conference Proceedings*, 151, 2015.